A Monte Carlo simulation study of branched polymers

Arun Yethiraj
Theoretical Chemistry Institute and Department of Chemistry, University of Wisconsin, Madison, Wisconsin 53706

(Received 24 October 2006; accepted 4 October 2006; published online 22 November 2006)

Monte Carlo simulations are presented for the static properties of highly branched polymer molecules. The molecules consist of a semiflexible backbone of hard-sphere monomers with semiflexible side chains, also composed of hard-sphere monomers, attached to either every backbone bead or every other backbone bead. The conformational properties and structure factor of this model are investigated as a function of the stiffness of the backbone and side chains. The average conformations of the side chains are similar to self-avoiding random walks. The simulations show that there is a stiffening of the backbone as degree of crowding is increased, for example, if the branch spacing is decreased or side chain length is increased. The persistence length of the backbone is relatively insensitive to the stiffness of the side chains over the range investigated. The simulations reproduce most of the qualitative features of the structure factor observed in experiment, although the magnitude of the stiffening of the backbone is smaller than in experiment.
 [DOI: 10.1063/1.2374884]

I. INTRODUCTION

Molecular bottle brushes are a relatively new class of polymer molecules where long side chains are grafted onto every monomer of a polymer backbone. One can envisage applications in the fabrication of nanostructures if the shape of the molecules can be controlled by tuning the nature of the side chains. There has been considerable recent interest in the conformational properties of these molecules and there have been several experimental and theoretical studies.[1–7] In this work we present a computer simulation study of isolated branched polymers composed of hard-sphere chains and investigate the effect of backbone and side chain flexibility on the conformational properties and static structure.

The basic idea is that the topological stiffness of the molecules, and hence its overall shape, can be controlled via the nature of the side chains, which are expected to form a dense brush. For short backbones, one can expect the backbone to collapse and the side chains to form a corona like a star polymer, but for longer backbones this is no longer favorable and the backbone is more likely to extend, with the side chains arranged transversely. For the molecules studied to date, there is no consensus regarding the shape of these polymers.

Most experimental systems consist of fairly flexible side chains grafted on to fairly flexible backbones. Examples are polystyrene (PS) or poly(methyl methacrylate) (PMMA) side chains on PS, PMMA, or poly(alkyl methacrylate) (PAMA) backbones.[3,5,6] All of these polymers have Kuhn lengths, l_K, (defined as $l_K \equiv \langle R^2 \rangle / R_m$, where $\langle R^2 \rangle$ is the mean-square end-to-end distance and R_m is the end-to-end distance at full extension) in the range of $l_K \approx 1.5-2$ nm. This corresponds to about 6 monomers; a fully flexible polymer composed of tangent freely jointed hard spheres has a Kuhn length that corresponds to about 4–5 monomers.

The conformational properties are inferred from scattering experiments. The quantity measured in small angle x-ray (SAXS), static and dynamic light scattering (SLS and DLS) and small angle neutron scattering (SANS) experiments is the static structure factor (or the form factor) of the molecules. In most cases, the conformational properties of the polymer *backbone* are not directly accessible because of problems with intensity. For example, although it is possible to selectively deuterate the backbone in order to obtain contrast in SANS, meaningful scattering intensities are only obtained for long backbones.[5] As a consequence, considerable analysis of the raw data is necessary in order to determine the conformational properties. The data are normally analyzed in terms of a semiflexible cylinder with a thickness due to the side chains.[3,6] The overall intensity is decomposed into a product of the scattering from the cylinder axis (which is not necessarily the polymer backbone) and scattering from the side chains, with some assumption for the cross-section density profile of the side chains about the cylinder. When scattering due to internal density fluctuations is taken into account, the scattering data can be fit to provide the conformational properties of the cylinder axis and the side chains.

There is some controversy regarding the shape of these molecules determined from experiment. Some experiments[1,4,6] suggest that the contour length of the cylinder per backbone monomer is independent of the degree of polymerization of the side chains, whereas others suggest that this contour length increases as the branch length is increased.[8] Experiments seem to agree, however, that the Kuhn segment length is significantly increased (by one or two orders of magnitude) compared to the bare backbone polymer. Some experiments, however, find a sharp transition between ellipsoidal and cylindrical conformations[3] while others suggest these molecules are self-avoiding walks on long length scales.[6] Given the complexity of the analysis, the

details of which are different in the different experimental groups, it is hard to determine the reason for these discrepancies in results.

There have been a number of theoretical studies of bottle-brush polymers[9–11] using self-consistent field theory and Flory-type theories. The theories predict that for long enough side chains the backbones will be stretched, and suggest the possibility of liquid crystalline phases for long side chains. These theories are appropriate for the case where the degree of polymerization of the backbone (N_b) is much larger than that of the side chains (N_s), with $N_s \gg 1$. As has been pointed out previously,[10,11] however, simulations (and probably experiments) are generally not in the scaling regime, making it difficult to test the predictions of the theories. It is not surprising, therefore, that the theoretical predictions for the dependence of the chain persistence length on the length of the side chains are not in agreement with experiment[6] or simulations.[10]

There have been several computer simulation studies of highly branched polymers, all of which have considered highly coarse-grained models of the polymers.[12–17] The majority of studies have focused on polymers with flexible backbones, although there have been a few studies that investigated the effect of the semiflexibility of the backbone and side chains.[14,17,18] With some notable exceptions,[14,18] in most of these studies the length of the side chains (about 5–10 beads) is much smaller than that in typical experiments (about 25–50 monomers). The simulation studies all agree that the incorporation of side chains leads to a stiffening of the backbone, although the degree of stiffening is much smaller than in experiments. Generally, the persistence length of the backbone increases by about a factor of 2 in the simulations, compared to about one or two orders of magnitude in the experiments. An exception is the study of Saariaho *et al.*,[14] who found an order of magnitude increase in the backbone persistence length when rigid rodlike 80 bead side chains were attached to every other bead of a flexible 300 bead backbone. Saariaho *et al.*, [18] showed that the intrinsic stiffness of the side chains affected the conformational properties of the backbone on local as well as global length scales. Recently Connolly *et al.*, [17] have emphasized the distinctions between topological stiffness and intrinsic stiffness, pointing out that the internal structure of a molecule with topological stiffness is quite different from a semiflexible wormlike chain.

There has not been much synergy between computer simulations and experiment. Only a handful of studies[14,18] have considered side chains that are as long as in the experimental systems. These studies were aimed at testing the theoretical predictions, and focused on the backbone persistence length, which is not measured directly in experiment.[6] What is lacking is a systematic study of the effect of various system parameters, e.g., backbone length, side chain length, branch spacing, on experimentally measured properties of branched polymers. This is the focus of the present work.

In this paper we report results of Monte Carlo simulations of isolated branched polymers. The backbone and side chains consist of tangent hard spheres and a bending potential is introduced in order to tune the stiffness of the backbone and the side chains. We investigate the effect of various system parameters on the conformational and structural properties, such as structure factor, radius of gyration, hydrodynamic radius, and asphericity, of these molecules. We find that increasing the "crowding" increases the stiffness of the polymer backbone. For example, increasing the length of the side chain or branch spacing causes the backbone to become stiffer compared to the linear chain. Increasing the stiffness of the side chain, however, decreases the crowding slightly as the side chains extend further away from the backbone, and this results in a slight decrease in the backbone stiffness compared to flexible side chains. The backbone is stiffened on intermediate length scales with self-avoiding walk behavior recovered on long length scales. The simulations contradict the idea[8] that the side chains behave like two-dimensional self-avoiding random walks. The stiffening of the backbone is smaller than what is seen in experiments. We therefore argue that the fully flexible or semiflexible model employed in this work (and all previous simulations) might miss some salient features of experimental systems.

The simulations results for the structure factor of the molecule are in qualitative agreement with recent experiments and support the approximations made in the experimental analysis.[6] The structure factor of the backbone can be fit by a worm-like chain model if the length of the chain is floated as an adjustable parameter in addition to the persistence length. If the total form factor is represented as a product of a backbone and a cross-section contribution, the estimates for the side chain radius of gyration and backbone persistence length are in good agreement with a direct measurement in the simulation.

The rest of the paper is organized as follows. The simulations are described in Sec. II, results are presented and discussed in Sec. III, and some conclusions are presented in Sec. IV.

II. MONTE CARLO SIMULATIONS

The polymer molecules are modeled as chains of hard spheres. The geometry of the molecules is depicted in Fig. 1. Each molecule consists of N_f equally spaced side chains of equal length, N_s, with the branch points separated by N_g beads along the backbone. When the spacing between side chains is nonzero, i.e., $N_g > 0$, the linear segments at the ends of the molecule contain N_g beads, and when $N_g = 0$ these segments contain one bead. The total number of sites, N, is given by $N = (N_g + N_s + 1)N_f + N_g$ for $N_g > 0$ and $N = (N_s + 1)N_f + 2$ for $N_g = 0$. The number of beads, N_b, along the backbone is given by $N_b = N - N_f N_s$. The bond length and hard-sphere diameter are fixed and set equal to σ, which is the unit of length. In addition, there is a bending potential, E_B, between adjacent bonds given by

$$\beta E_B = \varepsilon_i (1 + \cos\,\theta), \tag{1}$$

where β^{-1} is Boltzmann's constant multiplied by the temperature, θ is the bond angle, and the subscript i refers to either the side chain (ε_S) or the backbone (ε_B). Each branch is attached to the backbone in a freely jointed fashion.

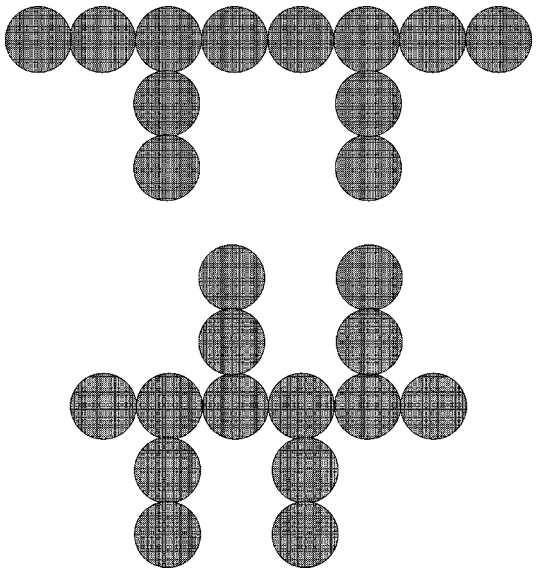

FIG. 1. Geometry of branched molecules with N_f side chains of length N_s separated by N_g beads along the backbone for $N_g=2$ (top) and $N_g=0$ (bottom). In the top molecule $N_f=2$ and in the bottom molecule $N_f=4$ ($N_s=2$ for both).

Initial configurations are generated with the backbone and side chains as rods, similar to Fig. 1, or from the final configuration of a previous simulation (for example, with a different stiffness) if available. Simulations proceed via attempts to change the conformation of the molecule via an extension of the pivot algorithm.[19] In our implementation each attempt consists of the following steps. First either a backbone or branch move is chosen randomly. If a backbone move is selected, one of the backbone atoms is chosen randomly as the pivot point. This divides the molecule into two parts, and the shorter of the two parts is rotated by a randomly chosen angle about one of the principle axes. If a branch move is selected, one of the side chains is chosen randomly and then one of the beads on that branch is selected (randomly) as the pivot point. The rest of the branch is then rotated about this bead by a randomly chosen angle about one of the principle axes. The move is accepted according to the Metropolis criterion.[20] For this model the pivot move efficiently samples configuration space as manifested in the decay of the end-to-end vector and radius of gyration autocorrelation functions.

The initial configuration is equilibrated before properties are averaged. In the equilibration stage the end-to-end vector and radius of gyration autocorrelation functions for the backbone and side chains are calculated to determine how many attempted moves are required for a statistically independent configuration. Properties are then averaged over of the order of 50 000 independent configurations. Simulations are performed in blocks of 10^6 moves with the final configuration of one block used as the initial configuration for the next. Statistical uncertainties are reported as one standard deviation of the variation of the mean over these blocks. A variety of conformational and structural properties are monitored, and are described in the next section.

TABLE I. Summary of simulation results for the persistence length of the backbone and the side chains.

N	N_g	N_b	N_s	ε_B	ε_S	l_p (backbone)	l_p (side chains)
601	1	101	10	0	0	10.5±0.2	2.84±0.02
601	1	101	10	0	5	11.2±0.2	8.68±0.04
601	1	101	10	5	0	17.2±0.4	2.76±0.02
601	1	101	10	5	5	19.3±0.4	8.56±0.06
1351	1	101	25	0	0	17.1±0.3	3.64±0.02
1351	1	101	25	0	5	16.8±0.4	10.90±0.06
1351	1	101	25	5	0	26.5±0.5	3.49±0.02
1351	1	101	25	5	5	30.3±0.8	10.5±0.1
2601	1	101	50	0	0	23.7±0.8	4.48±0.02
2601	1	101	50	0	5	20.6±1.4	12.4±0.2
2601	1	101	50	5	0	38.7±0.8	4.28±0.02
2601	1	101	50	5	5	40.7±1.2	11.76±0.16
2701	1	201	25	0	0	23.3±0.5	3.66±0.02
4051	1	301	25	0	0	26.4±0.6	3.66±0.02
5201	1	201	50	0	0	37.4±1.4	4.53±0.04
5201	1	201	50	0	5	39.8±2.0	12.40±0.20
5401	1	401	25	0	0	29.4±0.7	3.66±0.02
7801	1	301	50	0	0	44.3±2.4	4.54±0.02
10 401	1	401	50	0	0	49.4±2.5	4.55±0.02
2602	0	102	25	0	0	32±3	4.12±0.04
5202	0	202	25	0	0	47±4	4.12±0.02
7802	0	302	25	0	0	53±5	4.16±0.04
10 402	0	402	25	0	0	52±6	4.14±0.02

III. RESULTS AND DISCUSSION

The parameter space (N, N_s, N_g, ε_B, ε_S) is quite large and we restrict it by appealing to what is relevant to experimental systems. Since one bead in the coarse-grained model can correspond to either one or two monomers, we restrict ourselves to two values of N_g, i.e., $N_g=0$ and 1. This is motivated by the fact that in most experiments, the side chains are grafted to every monomer, i.e., every other carbon atom. We investigate three values of N_s, i.e., $N_s=10$, 25, and 50, which covers the range (25–50 monomers) in most experiments. We investigate values of ε_S and ε_B between 0 and 5. For linear tangent-hard-sphere chains, the Kuhn length varies from approximately 4 to 10 monomers over this range of the ε_B, which easily covers the range of stiffness in the experimental systems (about 6 monomers). Finally, we study the number of backbone beads ranging from 100 to 400. This is near the lower end of the experimental systems where the number of monomers in the backbone varies from 150 to 1000. In our choice of the number of backbone beads, we are limited by computational considerations because the total number of beads (N) becomes quite large given the size of the side chains. For example, for $N_g=0$, $N_f=400$, and $N_s=25$, $N=10\,402$. The systems studied are summarized in Table I.

A. Persistence length

An important measure of the stiffness of the polymer backbone is the persistence length, l_p, for which several definitions have been proposed in the literature. The classical

definitions are in terms of the projection of the end-to-end vector, **R**, on a bond vector, averaged over all conformations, i.e.,

$$l_k = \langle \mathbf{R} \cdot \mathbf{u}_k \rangle, \tag{2}$$

where $\mathbf{u}_k$ is the (normalized) bond vector between sites k and $k+1$. Flory[21] defined the persistence length as the average projection of **R** on an interior bond vector $\mathbf{u}_{\text{in}}$ far from any chain ends, while Yamakawa[22] defined the persistence length as l_1, i.e., the projection of **R** on the first bond. One can also define the persistence length in terms of the bond angle correlation function, $\langle \cos\theta(s) \rangle$, where θ is the angle between bond vectors separated by s segments along the backbone. For an ideal semiflexible chain $\langle \cos\theta(s) \rangle \sim \exp(-s/\lambda_C)$, where λ_C is a persistence length.

From an analysis of self-avoiding walks and branched polymers, we find that l_k is a strong function of k for $k < 100$ consistent with results of other simulations.[17] The qualitative behavior of l_1 and $l_{\text{in}} \equiv \langle \mathbf{R} \cdot \mathbf{u}_{\text{in}} \rangle$, where $\mathbf{u}_{\text{in}}$ is an internal bond, is similar, although the latter is larger by roughly a factor of 2. Either of these is a useful definition of l_p for our model. When the chain is flexible $\langle \cos\theta(s) \rangle$ does not decay exponentially except for large s. There is therefore some uncertainty in appropriate range of s where the exponential function should be fit. The persistence length obtained by this method is significantly larger than the other methods and is also a strong function of the degree or polymerization. For linear self-avoiding walks (SAWs) this method gives $\lambda_C = 11$, 23, and 31, and for $N = 101$, 203, and 407, respectively, which may be compared to $l_1 = 1.8$, 2, and 2.25, and $l_{\text{in}} = 4.1$, 4.7, and 5.3, for the same values of N. For chains that are sufficiently long and stiff, such an analysis of $\langle \cos\theta(s) \rangle$ is more meaningful and the results for the persistence length as similar to those obtained from the Flory definition, i.e., in this case $\lambda_C \approx l_{\text{in}}$.

For the purposes of comparing the stiffness of molecules with different length and spacing of branches, we define the persistence length, l_p, in terms of the wormlike chain. In this model,[23] the mean-square end-to-end distance, $\langle R^2 \rangle$, is given by

$$\langle R^2 \rangle = \frac{L}{\lambda} - \frac{1}{2\lambda^2}(1 - e^{-2\lambda L}), \tag{3}$$

where L is the contour length and λ is a parameter that characterizes the stiffness. We define the persistence length as twice the value of l_1 for this model, i.e.,

$$l_p \equiv \frac{1}{\lambda}(1 - e^{-2\lambda L}). \tag{4}$$

This definition is consistent with the results obtained from l_{in} for SAWs, i.e., $l_p = 3.8$, 4.4, and 4.8 for SAWs of length 101, 203, and 407, respectively. For the same lengths of SAWs, the Kuhn length $l_K = 3.7$, 4.3, and 4.8, respectively. Our definition of persistence length has the advantage that it is easily extracted from simulations, but has the disadvantage that it cannot be measured experimentally. We emphasize that we are not claiming that the polymer statistics are well fit by the wormlike chain model, but rather l_p is just a convenient and well-defined parameter to *characterize* the stiffness of the backbone or side chains.

The persistence length of the side chains is larger than that of an isolated chain of the same length, but is only weakly sensitive to the length or stiffness of the backbone. Table I lists the persistence lengths of the backbone and side chains for the simulations performed. In all cases the persistence length of a branch is higher than that of an isolated chain of the same length. For isolated linear SAWs ($\varepsilon_S = 0$) $l_p = 2.4$, 2.8, and 3.4 for $N = 10$, 25, and 50, respectively, which may be compared to $l_p = 2.84$, 3.64, and 4.48 obtained for side chains of the same length. Similarly, for isolated semiflexible SAWs with $\varepsilon_S = 5$, $l_p = 7.8$, 9.2, and 9.8 for $N = 10$, 25, and 50, respectively, which may be compared to $l_p = 8.7$, 10.9, and 12.4 for side chains of the same length and stiffness. For flexible side chains ($\varepsilon = 10$) the persistence length of the side chains is insensitive to the length of the backbone, and the increase in l_p (relative to an isolated chain) depends on the size of the side chains, going from about 18% for $N_s = 10$ to 36% for $N_s = 50$. A similar trend is observed for stiff side chains ($\varepsilon = 5$) with a slightly smaller percentage increase relative to an isolated chain, e.g., l_p increases by 6% for $N_s = 10$ to 30% for $N_s = 50$. Increasing the stiffness of the backbone results in a decrease in the persistence length of the side chains. This is because extending the backbone decreases the degree of crowding at the branch points.

The above trends can be understood in a qualitative fashion in terms of crowding effects. When the length of the side chains is increased, one expects the crowding effects to be stronger, since there are more beads near the backbone. This should cause the persistence length of the side chains to increase, as is observed. Similarly the crowding effects are weaker when either the side chains or the backbone is stiffer. For long backbones, one would not expect these crowding effects to depend on the length of the backbone, as is also observed in these simulations. Consistent with the above picture, the persistence length of the side chains increases when one goes from $N_g = 1$ to $N_g = 0$ for the same length of the backbone and side chains.

The crowding effects discussed above have a more significant impact on the persistence length of the backbone, and the stretching of the backbone can be significant. Figure 2 depicts the persistence length of the backbone as a function of the number of backbone beads for $\varepsilon_S = \varepsilon_B = 0$. As expected, the backbone l_p increases as N_b is increased. Over the range $100 < N_b < 400$, l_p increases by almost a factor of 2 for $N_g = 1$ and $N_s = 50$. This increase is larger than what is observed in SAWs and implies that the topological stiffness induced by the side chains is a strong function of N_b over the range investigated. The length of the side chains also has a significant effect on the backbone stiffness. Increasing N_s from 25 to 50 increases the backbone l_p by a factor of almost 2. In fact, for $N_g = 1$ and $N_b = 101$, the backbone persistence length increases in a roughly linear fashion with N_s in the admittedly limited range investigated.

The stiffness of the side chains has only a small effect on the topologically induced stiffness of the backbone. In most cases the backbone persistence length increases slightly

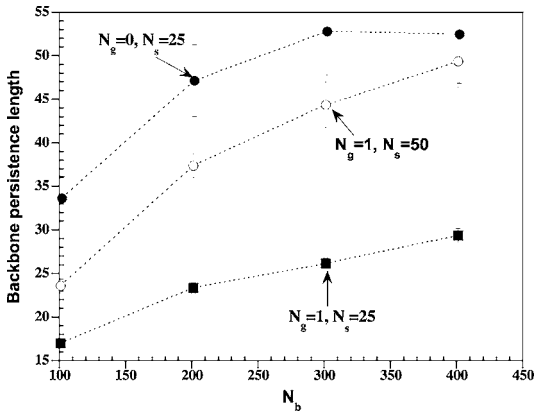

FIG. 2. Persistence length of the backbone as a function of number of backbone beads for various values of the branch length (N_s) and the number of beads between branch points (N_g) and for $\varepsilon_S=\varepsilon_B=0$. The lines are meant to guide the eye.

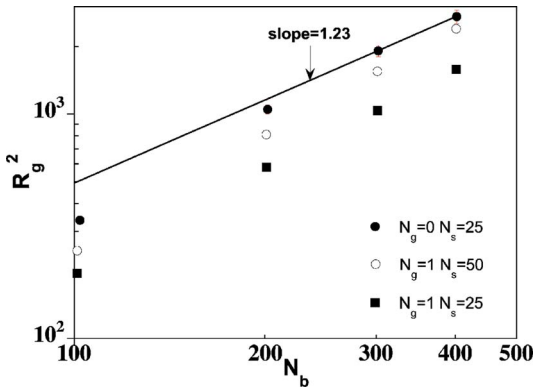

FIG. 4. Mean-square radius of gyration of the backbone as a function of number of backbone beads for various values of N_g and N_s. The solid line is a power-law fit to the last two data points for $N_g=0$ and $N_s=25$ with the slope as marked.

when ε_S is increased, but in some cases l_p decreases slightly (l_p decreases when ε_S is increased from 0 to 5 for $\varepsilon_B=0$, $N_b=101$, and $N_s=25$ and 50). Given the modest effect of stiffness, over the reasonable values of stiffness considered, only the fully flexible case ($\varepsilon_S=\varepsilon_B=0$) will be considered in the remaining sections.

In cases where l_{in} can be meaningfully extracted, the numerical values are similar to that presented for l_p, although the statistical uncertainties are much larger. For example, for $N_g=0$ and $N_s=25$, there is a plateau region in a plot of l_k versus k for $N_b \geq 200$, from which we extract values of $l_{\text{in}}=49$, 57, and 55 (±5 in all cases) for $N_b=202$, 302, and 402, respectively. Similarly, for $N_g=1$ and $N_s=50$ we obtain $l_{\text{in}}=40$, 49, and 53 (±5 in all cases) for $N_b=201$, 301, and 401, respectively. These values are similar to numerical values of l_p calculated from the wormlike chain model (see Table I).

In cases where λ_C can be extracted, the numerical values are higher than l_p and the dependence on the backbone length is weaker. Figure 3 is a semilog plot of $\langle \cos\theta(s)\rangle$ versus s for three cases. For $N_g=1$ and $N_s=50$ there is no linear regime for the shortest backbone ($N=2601$) but a clear linear regime is observed for longer chains (only $N=10\,401$ is shown in the figure). From the slope of the line for large s we extract values of $\lambda_C=67$, 78, and 80 (±10 in all cases) for $N_b=201$, 301, and 401, respectively. These numbers are larger than the values of l_p in Table I, and also a weaker function of N_b than l_p. For $N_g=0$ and $N_s=25$, the bond angle correlation function appears to display *two* roughly linear regimes, one for $s<80$ and another for $s>80$. A linear fit to the latter gives $\lambda_C=60$, 63, and 67 (±7 in all cases) for $N_b=202$, 302, and 402, respectively, although these numbers might not be reliable because there is not a single regime where $\langle \cos\theta(s)\rangle$ is exponential. Similar to what was seen for SAWs, the bong angle correlation function gives different estimates for the persistence length than other methods.

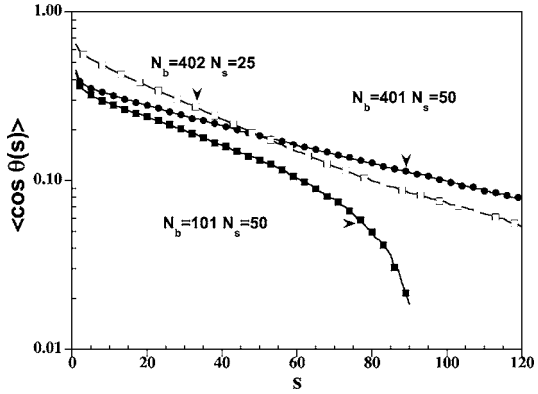

FIG. 3. Bond angle correlation function as a function of the number of segments separating the bonds. Filled and open symbols correspond to $N_g=1$ and $N_g=0$, respectively.

B. Molecular size and shape

The largest degree of polymerization studied in this work is too small for our molecules to be in the true scaling regime. An analysis of the chain size for the largest chains suggests, however, that the scaling of the backbone mean-square radius of gyration, R_g^2, with the degree of polymerization is consistent with that of a self-avoiding random walk. For a molecule with M sites, R_g^2 is defined as

$$R_g^2 = \frac{1}{M}\sum_{i=1}^{M} (\mathbf{r}_i - \mathbf{r}_{cm})^2, \tag{5}$$

where $\mathbf{r}_i$ is the position of site i and $\mathbf{r}_{cm}$ is the position of the center of mass. For the backbone, side chains, and molecule, M takes on the values of N_b, N_s, and N, respectively. Figure 4 depicts R_g^2 of the backbone as a function of N_b for various values of N_g and N_s on a logarithmic plot (for $\varepsilon_B=\varepsilon_S=0$). As expected, the size of the molecules is a strong function of the degree of crowding. In all cases, the data shows a slight curvature, although the data for the three highest values of N_b can be fit to a power law. A fit of this type gives an exponent of 1.41±0.05, 1.37±0.03, and 1.36±0.02 for ($N_g=1, N_s=50$), ($N_g=1, N_s=25$), and ($N_g=0, N_s=25$), respectively. In Fig. 2 the persistence length as a function of N_b did not show a plateau except for the two highest values of N_b for $N_g=0$. If we fit the R_g^2 data for these two cases to a power law, we obtain a slope of 1.23, which is consistent with the value expected for a SAW. One can understand the effective

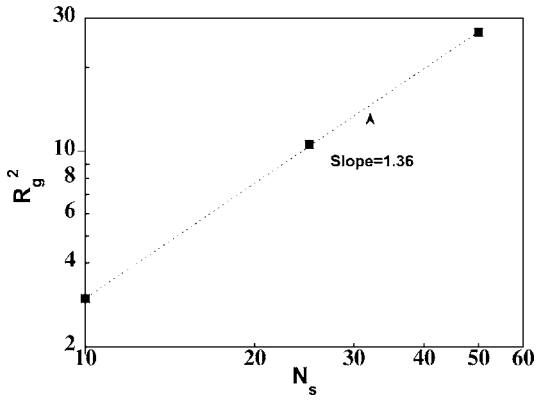

FIG. 5. Mean-square radius of gyration of the side chains as a function of the number of beads in the branch for $N_g=1$ and $N_b=101$. The dashed line is a power-law fit to the data with slope as marked.

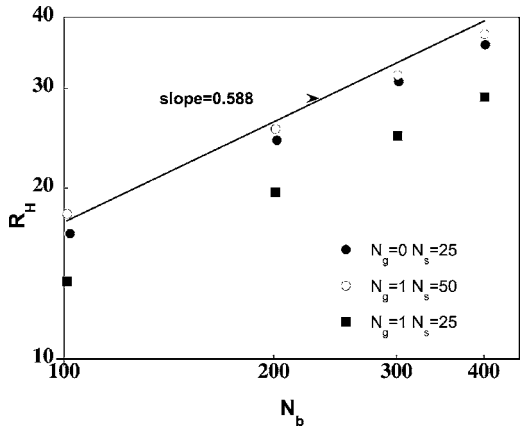

FIG. 6. Hydrodynamic radius as a function of the number of backbone beads for various values of N_g and N_s. The solid line is a power law with the slope as marked.

exponents of $\approx 1.35-1.4$ by noting that the chain is stretched on short-length length scales, which results in an increase in the exponent from that of a SAW toward that of a rod.

Over the limited range of N_s investigated, the size of the side chains scales in a power-law fashion with the number of beads, with an exponent that is higher than that of a SAW. Figure 5 depicts the average R_g^2 of the side chains for $N_b=101$ on a logarithmic plot. The data is well fit by a straight line with a slope of 1.36, which implies that $R_g^2 \sim N_s^{1.36}$. This scaling of the branch size with N_s is consistent with experiments[8] where a scaling exponent of 1.4 was reported. Since the scaling exponent for a two-dimensional SAW is 1.5, Fischer and Schmidt[8] suggested that the side chains might be essentially two dimensional. By representing the side chains in terms of an equivalent spheroid with the same moment of inertia tensor, we calculate the three semiaxis lengths. We find that the ratio of the two smaller lengths is approximately 3.3, which is close to that of a *three*-dimensional SAW. This demonstrates that the side chains are not two dimensional (which is obvious when one looks at snapshots of the conformations) but probably too short to be in the asymptotic scaling regime.

The scaling of the hydrodynamic radius with backbone length is consistent with SAW behavior. The hydrodynamic radius is defined as

$$\frac{1}{R_H} = \frac{1}{N^2} \sum_{i,j=1}^{N} \left\langle \frac{1}{r_{ij}} \right\rangle, \tag{6}$$

where r_{ij} is the distance between sites i and j. Figure 6 depicts R_H as a function of N_b on a logarithmic plot. Over the range of N_b investigated, the simulations are consistent with power-law behavior. Also shown is a power-law function with a slope of $\nu=0.588$, i.e., the SAW exponent, and the simulations are consistent with this slope. The ratio R_g/R_H is a roughly linear function of $N_b^{\nu-1}$ with $\nu=0.588$. The extrapolated intercept falls in the range of $R_g/R_H \approx 1.6-1.8$, which is also consistent with what is seen for a SAW.[24]

The shape of a macromolecule can be characterized by its asphericity, A_d. For a molecule with M sites, the shape tensor $\mathbf{T}$ (averaged over conformations) is given by[25]

$$T_{\alpha\beta} = \frac{1}{M} \sum_{i=1}^{M} \langle (r_{i,\alpha} - r_{cm,\alpha})(r_{i,\beta} - r_{cm,\beta}) \rangle, \tag{7}$$

where α and β are the Cartesian coordinates (x, y, and z), $r_{i,\alpha}$ is the α coordinate of the position of site i, and $r_{cm,\alpha}$ is the α coordinate of the center of mass of the molecule. The asphericity of the molecule can be defined as[25]

$$A_d = \frac{1}{2} \left\langle \frac{\sum_{i<j} (\lambda_i - \lambda_j)^2}{(\sum_i \lambda_i)^2} \right\rangle, \tag{8}$$

where the λ_i are the eigenvalues of $\mathbf{T}$. In the limiting cases of a sphere and a rod, $A_d=0$ and 1, respectively. For sufficiently long chains ($N>50$) $A_d \approx 0.37$ for random walks[25] and we find that $A_d \approx 0.45$ for freely jointed hard-sphere chains.

The average asphericity of the side chains is insensitive to the degree of polymerization, but that of the backbone and entire molecule is a strong function of the degree of polymerization. Figure 7 depicts A_d for the backbone, side chains, and entire molecule as a function of N_b for $N_g=1$ and $N_s=50$. A_d for the side chains is essentially constant, emphasizing that the conformation of the side chains is insensitive to the backbone length, although the side chains are more stretched than isolated self-avoiding random walks (A_d is

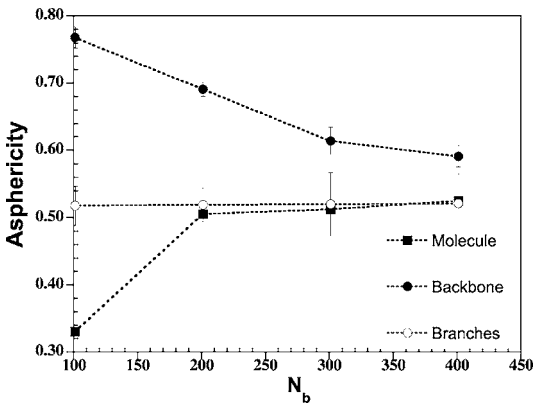

FIG. 7. Asphericity of the backbone, side chains, and the entire molecule as a function of the number of backbone beads for $N_g=1$ and $N_s=50$.

larger by about 10%). A_d for the backbone is a decreasing function of N_b while that of the entire molecule is an increasing function of N_b. These trends may be understood as follows. For semiflexible chains, when the chain length is smaller than the persistence length, A_d has a large value because the chain is persistent on these length scales. When the chain is many persistence lengths long, it can wrap around and this decreases the value of A_d. For the backbone, the ratio of the length to the persistence length is an increasing function of N_b (even though l_p increases) over the range of N_b investigated, and it is therefore reasonable that A_d decreases with increasing N_b. The presence of the side chains tends to decrease the A_d of the molecule relative to the backbone, and this effect is particularly important for short backbones. As a consequence, the asphericity of the molecule increases with increasing N_b.

C. Structure factor

An important experimentally measured quantity is the structure factor, $S(q)$, defined as

$$S(q) = \frac{1}{M}\left\langle \sum_{ij} e^{i\mathbf{q}\cdot\mathbf{r}_{ij}} \right\rangle, \tag{9}$$

where M is the number of sites, $\mathbf{q}$ is the momentum transfer variable, and $\mathbf{r}_{ij}$ is the vector between sites i and j. $S(q)$ is proportional to the scattering intensity, $I(q)$, measured in experiments. The form factor, $P(q)$, is defined as $P(q) \equiv S(q)/M$. For low values of the wave vector q, $S(q)$ reflects the behavior on length scales of the order of the size of the molecules $[S(q\to 0)=M]$, and for high values of q, $S(q)$ probes correlations on short length scales. The behavior of $S(q)$ in the scaling regime, i.e., $1 \ll q\sigma \ll qR_g$, can be understood by considering a correlation volume R with m beads. The intramolecular pair correlation function, $S(r)$, scales as $S(r)\sim m/R^3$. Since $R\sim m^{\nu}$, $S(r)\sim R^{1/\nu-3}$, which implies $S(q)\sim q^{-1/\nu}$. For an ideal chain, $\nu=1/2$ and a plot of $q^2S(q)$ versus q will show a plateau in the scaling regime. For a rod, $\nu=1$ and a plot of $qS(q)$ versus q will show a plateau in the scaling regime.

The simulation results for the structure factor are consistent with experiments.[6] Figures 8(a)–8(c) depict $S(q)$ as a function of q (on a logarithmic plot) for the molecule [denoted $S(q)$], backbone [denoted $S_b(q)$], and side chains [denoted $S_s(q)$], respectively, for $N_g=1$, $N_s=50$, and various values of N_b. We first consider the structure factor of the entire molecule, depicted in Fig. 8(a). For low wave vectors there is a plateau in $S(q)$ with a value equal to the number of scatterers (sites). For higher wave vectors $S(q)$ becomes independent of the degree of polymerization. At intermediate values of q there is a hint of scaling behavior consistent with a self-avoiding walk, manifested by a scaling close to that of the SAW (the solid straight line represents SAW behavior). At still higher wave vectors $S(q)$ is dominated by scattering from correlations between different side chains. Note that $S(q)$ does not display the q^{-1} regime, which has been interpreted to mean that the chain does not behave like a stiff cylinder on intermediate length scales.[6]

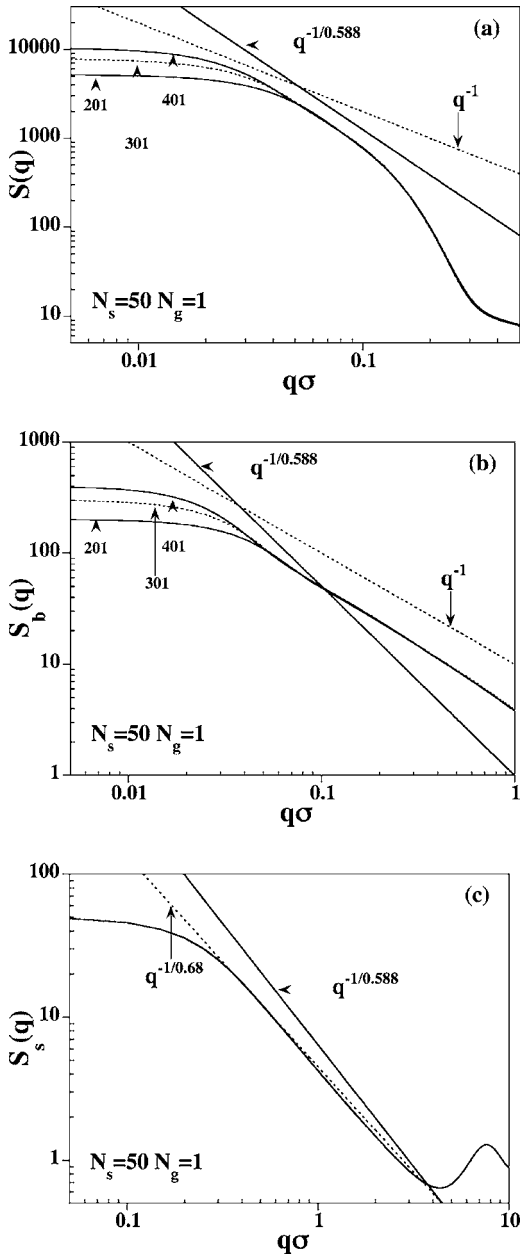

FIG. 8. Structure factor of the (a) molecule, (b) backbone, and (c) side chains for $N_g=1$, $N_s=50$, and various lengths of the backbone (as marked). The straight lines are power-law curves with exponents as shown. In (c) the curves for different values of N_b essentially superimpose and are indistinguishable from each other.

The structure factor of the backbone, however, does not follow that of a SAW on intermediate length scales, but displays behavior more consistent with that of a wormlike chain. Figure 8(b) depicts the structure factor of the backbone, denoted $S_b(q)$. In the intermediate scaling regime, $S_b(q)\sim q^{-1}$, suggesting that the backbone is rodlike on these length scales.

Figure 8(c) depicts the structure factor of the side chains, denoted $S_s(q)$. Note that $S_s(q)$ includes only correlations within each branch, and is averaged over all the side chains. $S_s(q)$ is essentially independent of N_b. In the scaling regime, $S_s(q)\sim q^{-1/0.68}$ to a good approximation, consistent with the scaling of $R_g\sim N_s^{1.36}$ (see Fig. 5). We reiterate that this scal-

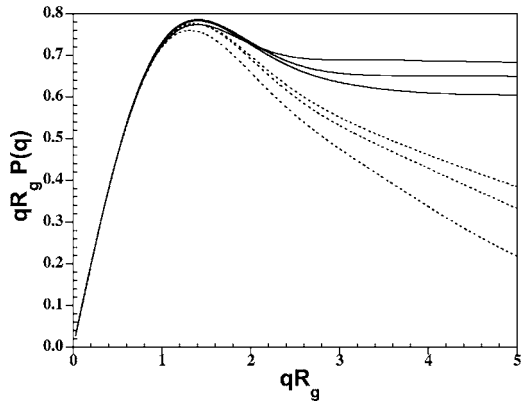

FIG. 9. Holtzer plot for the backbone (solid lines) and molecule (dashed lines). In each case, the lines correspond to (from top to bottom) N_b=401, 301, and 201.

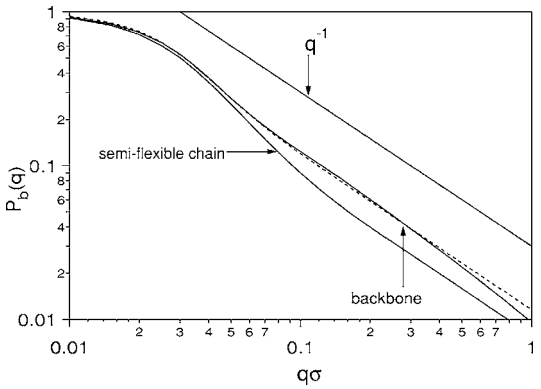

FIG. 10. Comparison of the structure factor of the backbone of a bottle brush (with N_b=401, N_g=1, and N_s=50) to an equivalent linear semiflexible chain with the same value of the mean-square end-to-end distance. The dashed line is a fit of the backbone structure factor to the wormlike chain model with both contour length and persistence length floated as adjustable parameters.

ing is not due to two-dimensional behavior, and that the principle semiaxis lengths of the side chains are consistent with that of three-dimensional SAWs.

Figure 9 depicts the form factor of the molecule (dashed lines) and the backbone (solid lines) on a so-called Holtzer plot, where $qR_gP(q)$ is plotted versus qR_g. On such a plot a rod would show a plateau region. Clearly the Holtzer plot for the molecules does not display any plateau, but that of the backbone has a plateau for the longest backbone. This is consistent with the backbone being stiff on intermediate length scales. Such behavior was not observed in simulations of chains with shorter side chains.[17]

Although it is possible, in principle, to measure the backbone and side chain form factors independently, using selective deuteration in SANS, for example, most experiments report the overall structure factor, $S(q)$. The form factor of the backbone and side chains is usually extracted via further analysis. We use the simulation results to test some of the approximations inherent to analyses of this nature. Rathgeber *et al.*,[6] for example, assumed a wormlike chain model for the backbone[26] and a Gaussian function for the transverse density profile of the side chains around the backbone. They assumed that the overall form factor could be factored into a product of a contribution from the backbone and a contribution from the cross section, i.e.,

$$P(q) \approx P_b(q)P_{\mathrm{CS}}(q), \tag{10}$$

where the cross-section form factor, $P_{\mathrm{CS}}(q)$, is the two-dimensional Fourier transform of the radial density profile. They fit the overall structure factor to this model (with additional contributions due to instrument resolution and internal fluctuations) to extract the persistence length of the backbone.

We find that the structure factor of the backbone differs from that of an equivalent semiflexible chain with the same number of beads. For a given bottle brush we obtain the structure factor of the equivalent semiflexible chain from Monte Carlo simulations of a single chain with N_s=0, N =N_b, and ε_B chosen (by trial and error) so that the semiflexible chain and the bottle brush have the same mean-square end-to-end distance. Figure 10 compares $P_b(q)$ for N_b=401, N_g=1, and N_s=25 to the equivalent linear semiflexible chain (with ε_B=24.5). The qualitative behavior of the two models is similar, and in both cases $P_b(q) \sim q^{-1}$ in the scaling regime. The quantitative differences are significant, however, by about a factor of 1.5–2 in the pertinent scaling regime.

It is instructive to fit $P_b(q)$ to the wormlike chain structure factor proposed by Pedersen and Schurtenberger[26] and used to analyze bottle-brush experiments.[6] If the contour length, L, is assumed to be the length of the backbone, then it is not possible to fit the data to the wormlike chain model. In this case the best fit to $P_b(q)$ is almost indistinguishable from the structure factor of the semiflexible chain depicted in Fig. 10, and the persistence length is $41.3 \pm 0.6\sigma$.

The wormlike chain fits the scattering data if the contour length is treated as an adjustable parameter. Floating L as a parameter is reasonable because the effective length of these cylinders can be shorter than the contour length of backbone.[8] If both the contour length, L, and the persistence length as adjustable parameters the structure factor can be fit to the wormlike model (dashed line in Fig. 10). For N_g=1 and N_s=50, we obtain $L=144\pm1\sigma$, $206\pm1\sigma$, and $272\pm1\sigma$ for N_b=201, 301, and 401, respectively. The corresponding values of the persistence length for these cases are $64\pm1\sigma$, $77\pm1\sigma$, and $85\pm1\sigma$. Interestingly, these values are close to the values of $\lambda_C=67\sigma$, 78σ, and 80σ, obtained by fitting the variation of the bond-angle autocorrelation function with distance along the backbone (see Fig. 3 and the associated discussion).

Figure 11 depicts $P_{\mathrm{CS}}(q) \equiv P(q)/P_b(q)$ on a logarithmic plot for N_g=0, N_s=25, N_b=402 (denoted A), N_g=1, N_s=50, N_b=401 (denoted B), and N_g=1, N_s=25, N_b=401 (denoted C). Dashed lines are Gaussian fits to the data for $q\sigma < 0.2$, and a good fit to the data is obtained. From the Gaussian fit, we extract cross section radii of gyration for these three cases to be 9.7σ, 6σ, and 6.5σ, respectively ($\pm 0.1\sigma$). One can also estimate the cross-section radius of gyration as twice the radius of gyration of this side chains. This gives values of 10.4σ, 6.5σ, and 6.7σ for the same three cases. These two sets of numbers are in excellent agreement with each other (within 10%), which suggests that this aspect of the analysis is sound.

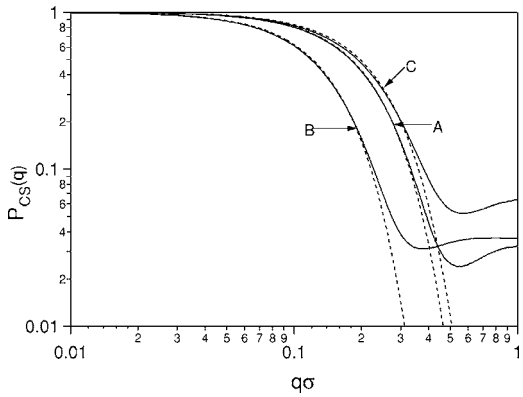

FIG. 11. Cross-section form factor (see text for definition) for $N_g=0$, $N_s=25$, $N_b=402$ (denoted A), $N_g=1$, $N_s=50$, $N_b=401$ (denoted B), and $N_g=1$, $N_s=25$, $N_b=401$ (denoted C). The dashed lines are Gaussian fits.

IV. CONCLUSIONS

Computer simulations are presented for the conformational properties and static structure of highly branched polymer molecules composed of freely jointed hard spheres. The focus of this work is to provide insight from simulations of a coarse-grained model but for experimentally relevant degrees of polymerization of the side chains and backbone. Most of the results are consistent with recent experiments. The side chains behave in a manner similar to self-avoiding walks, although the scaling of size with branch length and the scaling of the structure factor both suggest they are more stretched than SAWs. The conformational properties of the side chains are insensitive to the length of the backbone. On long length scales the molecules behave like self-avoiding walks, thus making the possibility of liquid crystal formation in melts or solutions of these molecules unlikely. An examination of the backbone structure, however, suggests that the backbone is stretched over intermediate length scales. This apparent contradiction can be resolved by noting that because of the bulky nature of the side chains, the molecule is not very aspherical on the length scale over which the backbone is stretched.

Visualization of snapshots of molecules are consistent with the above conclusions. Figure 12 depicts conformations of molecules for $N_g=0$, $N_s=25$, and $N_b=102$, 202, and 402. The molecule is locally stiff, over a length scale of the order of the persistence length, but for molecular weights relevant to experiment it wraps around significantly. These snapshots suggest that the name "bottle brush" might be a misnomer for these molecules, which might more appropriately called "caterpillar."[27]

Simulation results are presented for the static structure factor of the molecules, for experimentally relevant degrees of polymerization, and this allows us to evaluate the fitting methods used in experiments to determine the backbone and side chain dimensions. The simulations support the approximations used in experiment. For example, the factorization of the form factor into a backbone and cross-section contribution with a Gaussian approximation for the latter gives values for the cross-section radius of gyration that are in close agreement (within 10%) from what is obtained from the R_g of the side chains monitored in the simulations. A fit

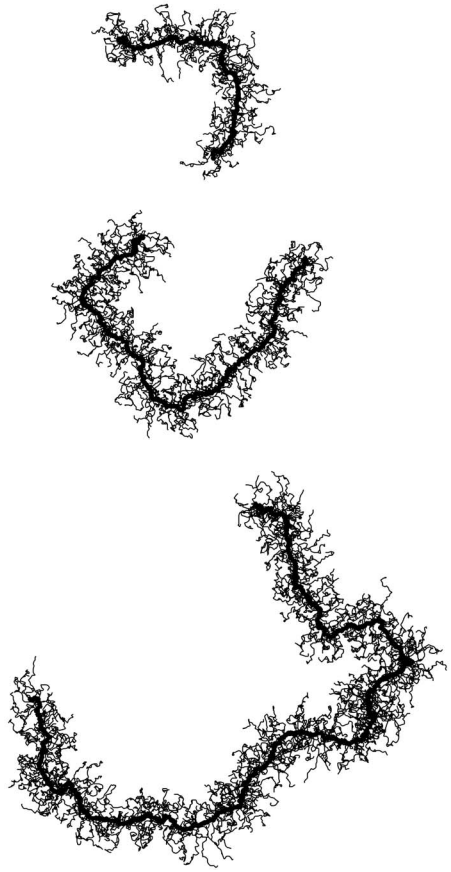

FIG. 12. Snapshot of conformations for $N_g=0$, $N_s=25$, and $N_b=102$, 202, and 402.

of the form factor of the backbone to the wormlike chain[26] gives persistence lengths that are in good agreement (5%–6%) with the values obtained from directly fitting the bond angle autocorrelation function. Such a fit also provides estimates for the length of the cylinder, which is not easily monitored directly in the simulations.

One important difference between these simulations and experiments is that the effective persistence length, i.e., topological stiffening due to the side chains, is significantly smaller in the simulations when compared to experiment. In the simulations, the persistence length of the backbone increases by about a factor of 10–12 relative to the linear chain, whereas in experiment the increase is by a factor of 30–100. The reason for this is not clear, but it is possible that this is related to the coarse-grained nature of the branch points in this model. In a real branched polymer, the branch cannot independently rotate about the branch point, i.e., rotation of a branch requires a "crankshaft" motion of the backbone. As a consequence, the steric hindrance due to the side chains is likely to be more significant in realistic chains than in the freely jointed case. One can also imagine that the tacticity of the branched polymer will play a significant role in real polymers. Going beyond the highly coarse-grained level is therefore an important step in the modeling of these materials. There are no such calculations in the literature, to our knowledge, and this is an important future direction.

ACKNOWLEDGMENTS

This material is based upon work supported by the National Science Foundation under Grant Nos. CHE-0315219 and CHE-0404704 (collaborative research in chemistry). I thank Prof. Dr. Manfred Schmidt and Professor Qiang Cui for useful discussions.

[1] N. Nemoto, M. Nagai, A. Koike, and S. Okada, Macromolecules **28**, 3854 (1995).
[2] M. Wintermantel, M. Gerle, K. Fischer, M. Schmidt, I. Wataoka, H. Urakawa, H. Kajiwara, and Y. Tsukahara, Macromolecules **29**, 978 (1996).
[3] M. Gerle, K. Fischer, S. Roos, A. H. E. Muller, M. Schmidt, S. S. Sheiko, S. Prokhorova, and M. Moller, Macromolecules **32**, 2629 (1999).
[4] K. Terao, T. Hokajo, Y. Nakamura, and T. Norisuye, Macromolecules **32**, 3690 (1999).
[5] S. Lecommandoux, F. Checot, R. Borsali, M. Schappacher, A. Deffieux, A. Brulet, and J. P. Cotton, Macromolecules **35**, 8878 (2002).
[6] S. Rathgeber, T. Pakula, A. Wilk, K. Matyjaszewski, and K. L. Beers, J. Chem. Phys. **122**, 124904 (2005).
[7] L. Feuz, F. A. M. Leermakers, M. Textor, and O. Borisov, Macromolecules **38**, 8891 (2005).
[8] K. Fischer and M. Schmidt, Macromol. Rapid Commun. **22**, 787 (2001).
[9] G. Fredrickson, Macromolecules **26**, 2825 (1993).
[10] A. Subbotin, M. Saariaho, O. Ikkala, and G. ten Brinke, Macromolecules **33**, 3447 (2000).
[11] A. Subbotin, R. Stepanyan, M. Saariaho, O. Ikkala, and G. ten Brinke, Macromolecules **33**, 6168 (2000).
[12] M. Saariaho, O. Ikkala, I. Szleifer, I. Erukhimovich, and G. ten Brinke, J. Chem. Phys. **107**, 3267 (1997).
[13] K. Shiokawa, K. Itoh, and N. Nemoto, J. Chem. Phys. **111**, 8165 (1999).
[14] M. Saariaho, A. Subbotin, I. Szleifer, O. Ikkala, and G. ten Brinke, Macromolecules **32**, 4439 (1999).
[15] M. Saariaho, O. Ikkala, and G. ten Brinke, J. Chem. Phys. **110**, 1180 (1999).
[16] S. Elli, F. Ganazzoli, E. G. Timoshenko, Y. A. Kuznetsov, and R. Connolly, J. Chem. Phys. **120**, 6257 (2004).
[17] R. Connolly, G. Bellesia, E. G. Timoshenko, Y. A. Kuznetsov, S. Elli, and F. Ganazzoli, Macromolecules **38**, 5288 (2005).
[18] M. Saariaho, A. Subbotin, O. Ikkala, and G. ten Brinke, Macromol. Rapid Commun. **21**, 110 (2000).
[19] N. Madras and A. D. Sokal, J. Stat. Phys. **50**, 109 (1988).
[20] N. Metropolis, A. W. Rosenbluth, M. N. Rosenbluth, A. H. Teller, and E. Teller, J. Chem. Phys. **21**, 1087 (1953).
[21] P. J. Flory, *Statistical Mechanics of Chain Molecules* (Wiley-Interscience, New York, 1969).
[22] H. Yamakawa, *Modern Theory of Polymer Solutions* (Harper & Row, New York, 1971).
[23] O. Kratky and G. Porod, Recl. Trav. Chim. Pays-Bas **68**, 1106 (1949).
[24] B. Dünweg, D. Reith, M. Steinhauser, and K. Kremer, J. Chem. Phys. **117**, 914 (2002).
[25] G. Gaspari, J. Rudnick, and A. Beldjenna, J. Phys. A **20**, 3393 (1987).
[26] J. S. Pedersen and P. Schurtenberger, Macromolecules **29**, 7602 (1996).
[27] R. S. Yethiraj, private communication (2005).